Synthesis of Ta₃N₅ Nanotube Arrays Modified with Electrocatalysts for Photoelectrochemical Water Oxidation
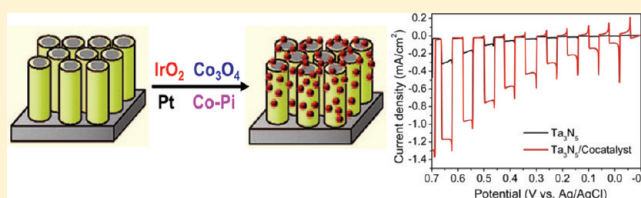
Yanqing Cong,[†,‡] Hyun S. Park,[‡] Shijun Wang, Hoang X. Dang, Fu-Ren F. Fan, C. Buddie Mullins, and Allen J. Bard*

Center for Electrochemistry, Department of Chemistry and Biochemistry, The University of Texas at Austin, 105 E. 24th St. Stop A5300, Austin, Texas 78712-1224, United States

Department of Chemical Engineering, Texas Materials Institute, Center for Nano- and Molecular Science, The University of Texas at Austin, 1 University Station C0400, Austin, Texas 78712-1224, United States

Ⓢ *Supporting Information*

ABSTRACT: Tantalum nitride (Ta_3N_5) is a promising material for photoelectrochemical (PEC) water oxidation with a narrow band gap (2.1 eV) that can effectively utilize visible light in the solar spectrum. Ta_3N_5 nanotube (NT) arrays were synthesized on a Ta foil by electrochemical anodization followed by an ammonia treatment at 800 °C. The photocurrent of nanostructured Ta_3N_5 was over 3 times higher than that of a dense regular Ta_3N_5 film in 0.1 M Na_2SO_4

aqueous solution at pH 11. Several electrocatalysts (IrO_2 nanoparticles (NPs), Co_3O_4 NPs, cobalt phosphate, and Pt NPs) were used to modify Ta_3N_5 NTs for PEC water oxidation. The photocurrent of Ta_3N_5 NTs modified with IrO_2 and Co_3O_4 was ca. four times higher than that of unmodified NTs. Cobalt phosphate also showed a positive improvement for PEC water oxidation on Ta_3N_5 NTs, whereas Pt was ineffective. Scanning electrochemical microscopy was used to measure the faradaic efficiency of the Ta_3N_5 photoanodes for water oxidation, which can reach as high as 88% for a Co_3O_4–Ta_3N_5 NTs photoanode, but is less than 15% at best, for Ta_3N_5 without the electrocatalyst. The results indicate that cobalt oxide and cobalt phosphate are promising candidates as electrocatalysts on Ta_3N_5 for water oxidation because Co is an earth-abundant material.

INTRODUCTION

We report the photoelectrochemical (PEC) performance of Ta_3N_5 nanotube (NT) arrays modified with several electrocatalysts for water oxidation. IrO_2 nanoparticles (NPs), Co_3O_4 NPs, cobalt phosphate, and Pt NPs were prepared as electrocatalysts of Ta_3N_5 NTs for water oxidation.

The generation of renewable clean energy is one of the most profound challenges of the 21st century.[1] Water splitting driven by solar energy into hydrogen and oxygen is a promising process for achieving renewable clean energy. Various semiconductors have been developed since Fujishima and Honda first suggested water splitting with TiO_2 under UV illumination in 1972,[2] and TiO_2 is one of the most studied semiconductors.[3−7] However, TiO_2 has a large band gap (3.0 eV for rutile and 3.2 eV for anatase) and can only perform efficiently under UV irradiation. Stable photocatalysts responsive to visible light are still few in number.

Recently, transitional metal (oxy)nitrides have attracted considerable attention as a new type of visible light-driven photocatalyst.[8−11] Among the metal (oxy)nitrides, tantalum nitride (Ta_3N_5) shows great promise with a narrow band gap (2.1 eV) that can utilize up to 600 nm visible light.[12] In addition, its conduction band edge and valence band edge positions are suitable for water splitting.[13] Ta_3N_5 powders and NPs have been developed for water oxidation in the presence of sacrificial reagents.[14,15] A 10% quantum efficiency for Ta_3N_5

under visible light irradiation (420 nm < λ < 600 nm) was obtained in a 0.01 M $AgNO_3$ aqueous solution.[16] Most recently, Yokoyama et al. have prepared a Ta_3N_5 thin film using a reactive sputtering technique. The anodic photocurrent of the film after NH_3 treatment increased by ca. 10 times relative to the untreated electrode at both 0.0 and 0.5 V versus Ag/AgCl in an aqueous solution containing $Fe(CN)_6^{3-}/Fe(CN)_6^{4-}$ as a redox couple.[9]

In addition to physicochemical properties, the PEC performance of a material also depends on the molecular-scale architecture and the nature of the active sites (cocatalyst). A NT array architecture can provide large surface area and sufficient lengths to effectively capture incident irradiation and improve the separation of photogenerated charge carriers.[17,18] Highly ordered metal oxide NTs on Ti,[5,19,20] Fe,[21,22] Ta,[23,24] Ti–Ru alloy,[25] and Ti–Fe alloy[26] have been successfully fabricated by the anodization method as a photocatalyst for solar energy applications. Feng et al. have prepared highly oriented Ta_3N_5 NT films by electrochemical anodization of a Ta foil followed by nitridation. The incident photon-to-current conversion efficiency (IPCE) at a wavelength 450 nm for 240 nm long Ta_3N_5 NTs reached 5.3% in 1 M KOH solution with

0.5 V bias.[17] However, at 0 V bias, the IPCE at wavelength 450 nm of 750 nm long Ta_3N_5 NTs decreased to ~0.4%. In any case, the PEC performance of Ta_3N_5 NTs has not yet been systematically studied. For water splitting, the oxygen evolution reaction (OER) and hydrogen evolution reaction are the two main electrochemical half reactions and the OER is more complicated because it involves a four electron, four proton transfer process with oxygen−oxygen bond formation. It occurs at significant overpotentials even with good electrocatalysts.[27] The valence band potential edge of Ta_3N_5 NTs is not sufficiently positive on account of its small band gap. Therefore, it is difficult to use Ta_3N_5 NTs alone as a photoanode for rapid OER. A suitable electrocatalyst could decrease the activation energy and provide active sites for water oxidation. In electrochemical systems, IrO_2,[28,29] Co_3O_4,[30,31] Co-phosphate (Co-Pi),[32,33] RuO_2,[34,35] Pt,[36,37] and Ni oxide[38,39] have been reported to be good electrocatalysts for water oxidation. However, the study of electrocatalysts as the cocatalysts of semiconductor photoelectrodes for PEC water oxidation is still limited.[27] Domen's group has reported the loading of IrO_2 NPs onto TaON and Ta_3N_5 films. IrO_2 modification could significantly increase the photocurrent for water oxidation and partially suppress the self-oxidation of TaON and Ta_3N_5 films.[9,11] Although IrO_2 is a good electrocatalyst for PEC water oxidation, iridium is one of the least abundant metals on earth and is not suitable for use on a very large scale.[40] Thus, it is desirable to explore other electrocatalysts that enhance the PEC performance of the Ta_3N_5 photocatalyst.

■ EXPERIMENTAL SECTION

Materials. $Co(NO_3)_2$ (99.999%), ferrocenemethanol (97%), NH_4F (99.99%), $NaBH_4$ (99%), sodium citrate (99.76%), Na_2SO_4 (99.0%), $(NH_4)_6Mo_7O_{24}\cdot4H_2O$ (99.98%) (Sigma-Aldrich, St. Louis, MO), H_2PtCl_6 (99.9%), K_2IrCl_6 (Ir 39%), VCl_3 (99%) (Alfa Aesar, Ward Hill, MA), Co-$(CH_3COO)_2\cdot4H_2O$, NaH_2PO_4 (99.5%), Na_2HPO_4 (99.9%), NaOH (97%), HNO_3 (65%), H_2SO_4 (95%), $(NH_4)_2SO_4$, ethylene glycol (99%), glycerol (99.5%), acetone (99.5%), ethanol (99.5%), and ammonium hydroxide (28%) (Fisher Scientific, Pittsburgh, PA) were all used as received. Bi-$(NO_3)_3\cdot5H_2O$ (99.999%) and $(NH_4)_{10}H_2(W_2O_7)_6\cdot xH_2O$ (99.99%) were obtained from Strem Chemicals (Newburyport, MA). Milli-Q DI water was used to prepare aqueous solutions. Ta foil (Alfa Aesar, 99.95% purity) was used as a substrate and cut into 15×15 mm^2 pieces to prepare Ta_2O_5 nanotube arrays. Anhydrous ammonia gas (Praxair, 99.995% purify) was used as received. A Au ring fiber disk electrode (RDE) coated on an optical fiber (SFS200/200G, Fiberguide Industries, Inc., Long Hill, NJ) was used to detect oxygen generated (Figures S1 and S7 of the Supporting Information for a more detailed description).

Preparation of Photoelectrodes. The Ta_3N_5 NTs were prepared by electrochemical anodization of a Ta foil followed by annealing in ammonia gas. The anodization was carried out according to a reported procedure.[23] Ta foil was cleaned by sonicating in acetone, ethanol, and DI water, and then dried in air. A mixed solution of ethylene glycol (5 vol %)/glycerol (100 vol %) combined with 0.2 M NH_4F and 0.15 M $(NH_4)_2SO_4$ was prepared as the anodization electrolyte. The pretreated Ta foil was anodized at constant voltage (20−30 V) for 3 h at room temperature to obtain Ta_2O_5 NTs. The as-formed Ta_2O_5 NTs were then annealed in a tube furnace at 800 °C under

anhydrous ammonia gas with a flow rate of 100 mL/min for 3 h to obtain Ta_3N_5 NTs.

For comparison, a Ta_3N_5 film was also prepared via a two-step process: first, a Ta_2O_5 layer of about 2 μm was grown by heating a similar Ta foil (without electrochemical anodization) at 500 °C for 30 min in air; then the Ta_2O_5 layer was annealed at the same nitridation conditions to convert Ta_2O_5 into a Ta_3N_5 film.

The W/Mo-doped $BiVO_4$ electrode was prepared as a control photoanode in the tip collection (TC)/substrate generation (SG) mode of scanning electrochemical microscopy (SECM). A 20 μM $(NH_4)_{10}H_2(W_2O_7)_6\cdot xH_2O$, 80 μM $(NH_4)_6Mo_7O_{24}\cdot4H_2O$, 4.2 mM $Bi(NO_3)_2\cdot5H_2O$, and 5 mM VCl_3 in ethylene glycol solution was prepared. The fluorine-doped tin oxide (FTO, TEC 15, Pikington, Toledo, OH) used as the substrate for the W/Mo-doped $BiVO_4$ electrode was washed and ultrasonicated for 30 min in an ethanol solution. Then, 100 μL of the precursor solution was drop-cast onto the FTO substrate. The film was annealed at 500 °C for 3 h under air atmosphere. The temperature was ramped from room temperature to 500 °C over 9 h.

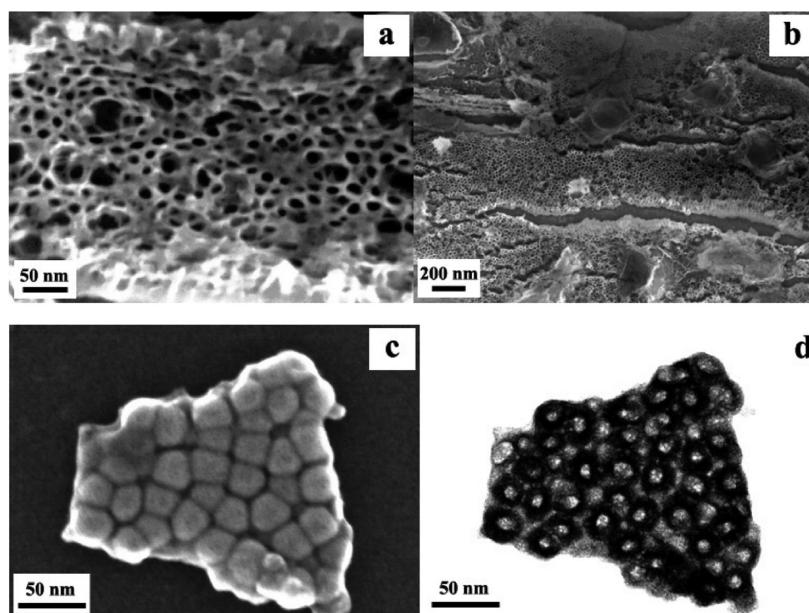**Preparation of Electrocatalyst on the Ta_3N_5 NT Arrays.** IrO_2, Co_3O_4, Co-Pi, and Pt electrocatalysts were prepared and loaded on the Ta_3N_5 NTs, respectively.

An IrO_2 colloidal solution was prepared by hydrolysis of K_2IrCl_6 in a basic aqueous solution.[11] A K_2IrCl_6 solution was adjusted to pH 12 using NaOH solution, and then heated at 70 °C for 30 min. After cooling to room temperature, the solution was adjusted to pH 9 using HNO_3 solution to obtain an IrO_2 colloidal solution. The Ta_3N_5 NTs were then soaked in the IrO_2 solution for 3 h. The resulting films (represented as Ta_3N_5 NTs/IrO_2) were rinsed with DI water and dried in air at room temperature.

Co_3O_4 NPs were synthesized following a previous procedure.[31] $Co(CH_3COO)_2\cdot4H_2O$ (0.50 g) was dissolved in ethanol (25.0 mL), and then 25% ammonium hydroxide (2.5 mL) was added under vigorous stirring. After stirring for 10 min, the solution was transferred into an autoclave (50.0 mL), sealed, and maintained at 150 °C for 3 h. After this, the autoclave was naturally cooled to room temperature. The resulting black solid products were washed with ethanol and the Co_3O_4 NPs were obtained. The Ta_3N_5 NTs were immersed in the Co_3O_4 NP solution for 3 h at room temperature, then washed with DI water, and dried in air to obtain films, represented as Ta_3N_5 NTs/Co_3O_4.

Co-Pi electrocatalyst films were prepared by electrochemical deposition.[32] The Ta_3N_5 NT arrays were exposed to a freshly made 0.5 mM $Co(NO_3)_2$ solution in 0.1 M sodium phosphate buffer (pH 7). A constant potential (1.4 V vs Ag/AgCl) was applied to deposit the Co-Pi on the surface of Ta_3N_5 NTs for 30 min. The resulting film (represented as Ta_3N_5 NTs/Co-Pi) was then rinsed with copious DI water.

Pt NPs were synthesized by using $NaBH_4$ to reduce H_2PtCl_6 precursor in the presence of sodium citrate.[41,42] 2 mM H_2PtCl_6 (40 mL) was mixed with 40 mM sodium citrate (2.4 mL), which served as the stabilizer. Fresh sodium borohydride solution (100 mM, 4.8 mL) was dropwise added into the mixed solution under vigorous magnetic stirring, and then the solution was stirred for 30 min at room temperature. The Ta_3N_5 NTs were soaked in the Pt NP solution for 3 h, then washed with DI water, and dried in air to obtain a film, represented as Ta_3N_5 NTs/Pt.

Figure 1. FESEM and TEM images of as-formed Ta_2O_5 NTs anodized at 20 V for 3 h at room temperature. (a) Top-view SEM at higher magnification. (b) Top-view SEM image at low magnification. (c) Bottom-view SEM image of a mechanically scratched-off as-formed Ta_2O_5 NT sample. (d) Bottom-view TEM image of the same piece of sample.

Characterization. The structure and morphology of the films were characterized using a field-emission scanning electron microscope (Hitachi S-5500 FESEM equipped with STEM). The X-ray diffraction (XRD) measurements were performed with a Bruker-Norius D8 advanced diffractometer using a Cu Kα radiation source operated at 40 kV and 40 mA with an incidence angle of 0.5 degrees. X-ray photoelectron spectroscopy (XPS) was acquired using a Kratos Axis Ultra DLD instrument (Manchester, UK) with a monochromatic Al X-ray source. UV−vis diffuse reflectance spectra were collected using a Cary 500 UV−vis NIR spectrophotometer with Labsphere DRA-CA-5500.
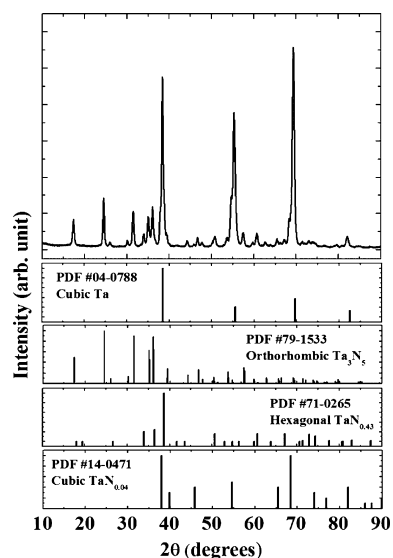
Photoelectrochemical Experiments. Ta_3N_5 NTs with or without deposited electrocatalyst films were used as working electrodes to measure their PEC properties. The PEC experiments were carried out in a three-electrode borosilicate glass cell equipped with a Pt-gauze counter electrode and an Ag/AgCl reference electrode. A potentiostat (CH Instruments, model 630D, Austin, TX) was used to perform electrochemical measurements. For TC/SG measurements, a SECM (Model 900B, CH Instruments, Austin, TX) was used. The geometric area of the working electrodes exposed to electrolyte solution and light irradiation was 0.2 cm^2. The electrolyte solution was 0.1 M sodium sulfate with pH adjusted to 11 by adding NaOH solution. A Xe lamp (XBO 150 W, Osram, Munich, Germany) provided the light irradiation with an incident UV−vis light intensity of about 110 mW/cm^2 through the electrolyte solution. An UV cutoff filter ($\lambda > 420$ nm) was used for visible light irradiation and the resulting visible light intensity is ca. 100 mW/cm^2. IPCE was measured through a monochromator (Photon Technology International, Birmingham, NJ) in combination with a power meter (Model 1830-C, Newport, Irvine, CA) and a silicon detector (Model 818-UV, Newport, Irvine, CA). Electrochemical impedance spectroscopy (EIS) was performed using an Autolab instrument (PGSTAT30/FRA2) to obtain the Mott−Schottky plot at

frequencies of 200, 500, and 1000 Hz and a peak-to-peak amplitude of 5 mV at each potential.

Digital Simulations. Electrochemical simulations were done using *COMSOL Multiphysics* v.3.5 software (Burlington, MA). The simulations domain and electrode configurations were set as shown in Figure S1 of the Supporting Information. A constant flux of 1.75×10^{-5} mol/m^2·s of the product generated from the substrate was used to simulate the OER at the photoanode. The diffusion coefficient of oxygen was taken as 2×10^{-9} m^2/s in an aqueous solution. The rate constant at the tip was assumed to be 0.1 m/s in the calculations. The tip potential bias was set at a potential negative of 0 V with the standard redox potential of 0.34 V versus Ag/AgCl for the reactant at pH 11. The large rate constant at a more negative potential at the tip was used to ensure the diffusion limited collection of oxygen at RDE. Simulations were done to study the TC/SG mode of SECM with various different distances between the tip and the substrate. Theoretical collection efficiency, η_{th}, that is, the ratio of the tip (collection) current and the substrate (generation) current was then calculated.
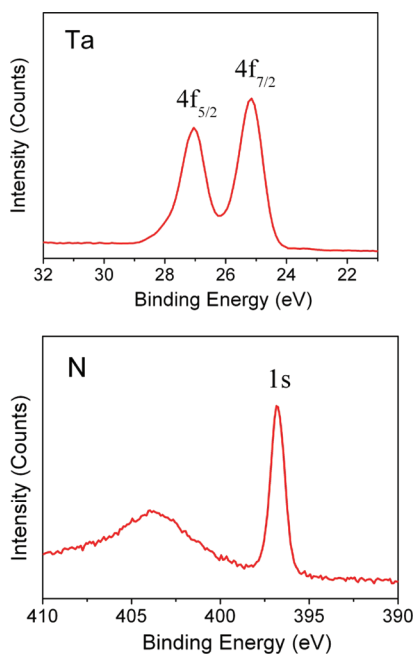
■ RESULTS AND DISCUSSION

Characterization of Ta_3N_5 NT Arrays. Figure 1 shows the FESEM and TEM images of an as-formed Ta_2O_5 NT sample anodized at 20 V for 3 h in a mixed solution of ethylene glycol (5 vol %)/glycerol containing 0.2 M NH_4F and 0.15 M $(NH_4)_2SO_4$ at room temperature. The bottom-view FESEM and TEM images were carried out on mechanically scratched-off samples. Ta_3N_5 NTs are open at the top surface and closed at the bottom layer. The average inner diameter of our nanotubes is 12 nm, their average outer diameter is 23 nm, and the length is ∼40 nm. Figure 2 shows the XRD patterns of Ta_3N_5 NTs nitrided for 3 h at 800 °C in a NH_3 flow. The main phase of Ta_3N_5 NTs was identified to be the orthorhombic-phase. Some intermediate phases (hexagonal-phase $TaN_{0.43}$ and cubic $TaN_{0.04}$) were also formed. Because Ta foil was used as the substrate, its XRD pattern was also detected. The surface

Figure 2. XRD patterns of Ta_3N_5 NTs nitrided for 3 h at 800 °C in a NH_3 flow: Representative diffraction pattern of the as-grown Ta_3N_5 NTs sample (upper) and several standard JCPDS patterns of different tantalum nitride forms (lower).

composition of Ta_3N_5 NTs was analyzed by XPS measurements and the results are shown in Figure 3. The Ta4f and N1s peaks
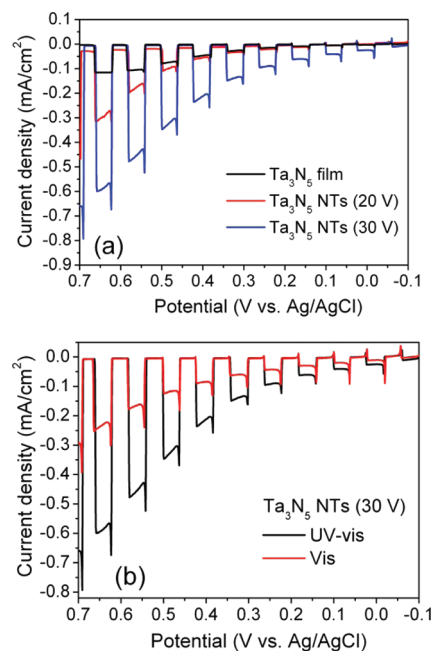

Figure 3. XPS spectra of Ta_3N_5 NTs. Ta_3N_5 NTs were prepared by nitriding a Ta_2O_5 NT in a tube furnace at 800 °C under a NH_3 gas flow of 100 mL min^{-1} for 3 h. The Ta_2O_5 NTs were prepared by anodizing a Ta foil at 20 V in a mixed solution of glycerol and ethylene glycol (5 vol %) containing 0.2 M NH_4F and 0.15 M $(NH_4)_2SO_4$.

indicate the presence of the corresponding elements in Ta_3N_5 NTs. The C1s peak (285.2 eV) was used as a standard to calibrate the binding energies. The Ta4f7/2 and Ta4f5/2 peaks appear at 25.2 and 27.1 eV, and the N1s peak appears at 396.8 eV. These energy values are coincident with Ta^{5+} and N^{3-} in Ta_3N_5 as reported by Domen's group.[43] The measured atomic

ratio of N to Ta from the XPS spectra of Ta_3N_5 NTs is ca. 1.4. This result is close to the stoichiometry of 1.67 for Ta_3N_5.

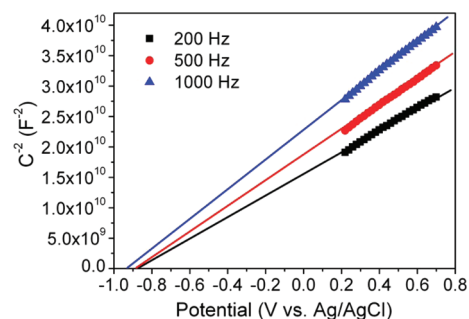**Photocatalytic Activity of Ta_3N_5 NTs.** The PEC performance of Ta_3N_5 NTs was studied using linear sweep voltammetry (LSV) in 0.1 M Na_2SO_4 aqueous solution with pH adjusted to 11. Part a of Figure 4 shows the LSVs of a Ta_3N_5 film (prepared

Figure 4. LSV of (a) Ta_3N_5 film prepared by nitriding a Ta_2O_5 layer formed on Ta foil, Ta_3N_5 NTs anodized at 20 and 30 V respectively for 3 h at room temperature under chopped UV−vis light irradiation; (b) Ta_3N_5 NTs anodized at 30 V for 3 h under chopped UV−vis and visible light ($\lambda > 420$ nm) irradiation. Electrolyte solution: 0.1 M Na_2SO_4 aqueous solution with pH adjusted to 11 by adding NaOH solution. Scan rate, 20 mV/s; light intensity, 110 mW/cm^2 (150 W Xe lamp).

by nitriding a Ta_2O_5 layer formed by heating the Ta foil at 500 °C for 30 min in air) and Ta_3N_5 NTs (synthesized by nitriding a Ta_2O_5 NTs film anodized at different voltage for 3 h at room temperature). Both Ta_3N_5 film and Ta_3N_5 NTs had anodic photocurrents under irradiation. The Ta_3N_5 NTs exhibited a photocurrent more than 3 times higher than the Ta_3N_5 film at 0.6 V versus Ag/AgCl in 0.1 M Na_2SO_4 aqueous solution (pH 11). The photocurrent of the Ta_3N_5 NTs showed a dependence on the anodization voltage used for the NTs synthesis. Ta_3N_5 NTs anodized at 30 V generated a photocurrent density of $\sim$0.6 mA/cm^2 under irradiation at 0.6 V versus Ag/AgCl, which was ca. twice of that for Ta_3N_5 NTs anodized at 20 V. The improvements were even larger in the region of less positive potentials. The nitridation at 800 °C under anhydrous ammonia gas with a flow rate of 100 mL/min for 3 h does not substantially change the morphology of Ta_2O_5 NTs (Figure S2 of the Supporting Information). The NT layers were uniform and stable. The average inner diameter of Ta_3N_5 NTs anodized at 30 V was ca. 14 nm and the length was ca. 1 μm. The current density during the anodization process had an important effect on the length of the Ta_3N_5 NT. Part b of Figure 4 shows the LSV of Ta_3N_5 NTs anodized at 30 V for 3 h under chopped UV−vis and visible light irradiation. About 43% of the photocurrent was contributed from visible light ($\lambda > 420$ nm) irradiation.

Mott−Schottky Plots. Ta_3N_5 NTs were analyzed by electrochemical impedance spectroscopy. Experiments were carried out in 0.1 M Na_2SO_4 solution (pH 11) at 200, 500, and 1000 Hz in the dark. The Mott−Schottky (MS) plots of Ta_3N_5 NTs ($1/C^2$ vs potential, where C is the capacitance of the semiconductor electrode) are shown in Figure 5. In the ideal

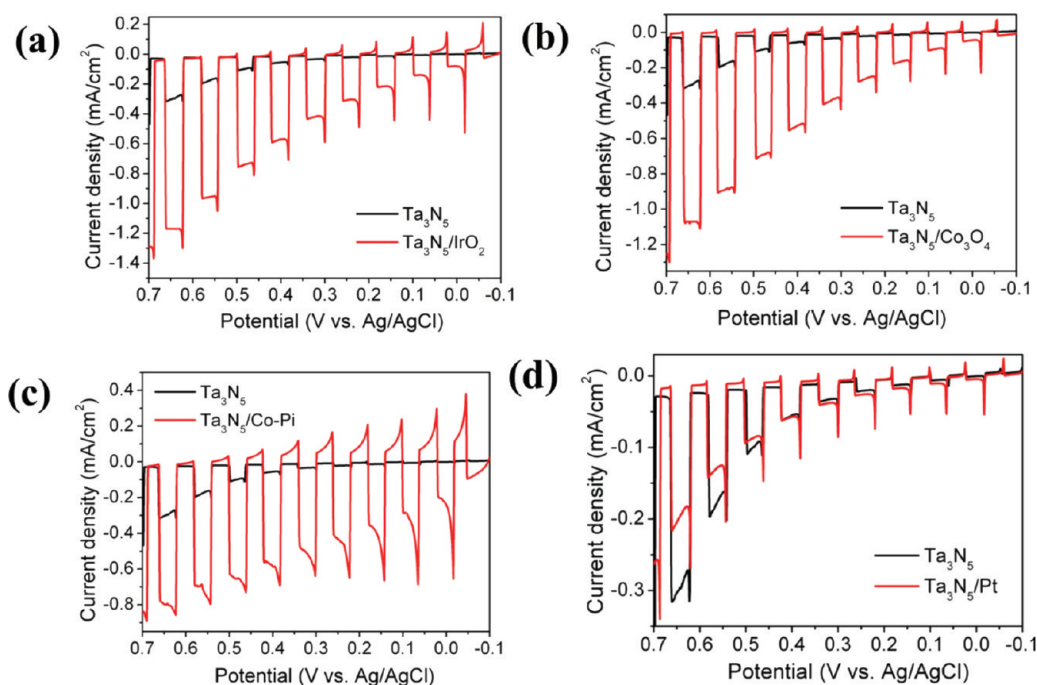**Figure 5.** Mott−Schottky plots of Ta_3N_5 NTs in 0.1 M Na_2SO_4 aqueous solution (pH 11) in the dark with an ac amplitude of 5 mV at each potential.

case, MS plots should be linear, providing information on the doping density and the flat band potential (E_{fb}) of the semiconductor. The E_{fb} of Ta_3N_5 was reported to be ca. −0.05 V versus NHE at pH 0 and shifted negatively with pH by 60 mV per pH unit change in the solution.[43] Thus, the E_{fb} of Ta_3N_5 NTs in 0.1 M Na_2SO_4 solution (pH 11) was estimated to be −0.93 V versus Ag/AgCl. As shown in Figure 5, the MS plots of a Ta_3N_5 NT electrode synthesized here, in spite of its porosity, exhibit positive slopes indicating that it is an n-type semiconductor. The E_{fb} of the Ta_3N_5 NTs, estimated from the

intercepts of the MS plots is about −0.9 V versus Ag/AgCl, which is consistent with the calculated E_{fb} value. Note that the MS plots show some frequency dispersion whose origin is not yet understood and requires further investigation.

PEC Measurements of Ta_3N_5 NTs/IrO_2. To decrease the activation energy of water oxidation, electrocatalysts were loaded on Ta_3N_5 NTs and the PEC performance of modified NT photoanodes was investigated. Part a of Figure 6 shows a comparison of LSVs of Ta_3N_5 NTs and Ta_3N_5 NTs/IrO_2 under chopped irradiation in 0.1 M Na_2SO_4 solution (pH 11) without the use of sacrificial reagents. The size of prepared IrO_2 NPs is ca. 16 nm in diameter (Figure S3 of the Supporting Information). The amount of IrO_2 loaded on Ta_3N_5 NTs was around 1.5 wt % as measured by the absorbance change of the IrO_2 solution at 600 nm. The photocurrent of Ta_3N_5 NTs/IrO_2 was ca. 4 times higher than that of Ta_3N_5 NTs at 0.6 V versus Ag/AgCl in 0.1 M Na_2SO_4 solution (pH 11). This indicated that IrO_2 was a positive OER electrocatalyst for Ta_3N_5 photoanode and could significantly improve water oxidation of Ta_3N_5 NTs under irradiation.

PEC Measurements of Ta_3N_5 NTs/Co_3O_4. Despite the good performance of IrO_2 as a electrocatalyst on Ta_3N_5 photoanode, Ir is one of the least abundant metals on earth and it is necessary to develop other electrocatalysts. Co is a promising candidate because it is an earth-abundant element and cobalt oxide is a good electrocatalyst for water oxidation in electrochemical systems. Co_3O_4 NPs were prepared for addition to the Ta_3N_5 NTs. The size of the prepared Co_3O_4 NPs is ca. 8 nm in diameter (Figure S4 of the Supporting Information), and the amount of deposited Co_3O_4 was around 1.7 wt % with respect to Ta_3N_5 NTs. Part b of Figure 6 shows the comparison of LSVs of Ta_3N_5 NTs and Ta_3N_5 NTs/Co_3O_4 under chopped irradiation in 0.1 M Na_2SO_4 solution (pH 11)

Figure 6. LSVs of Ta_3N_5 NTs/IrO_2 (a), Ta_3N_5 NTs/Co_3O_4 (b), Ta_3N_5 NTs/Co-Pi (c), and Ta_3N_5 NTs/Pt (d) in 0.1 M Na_2SO_4 solution (pH 11) under chopped irradiation. LSV of Ta_3N_5 nanotubes (NTs) is shown (black line) as a control sample. Scan rate, 20 mV/s; light intensity, 110 mW/cm^2 (150W Xe lamp). Ta_3N_5 NTs were prepared by nitriding a Ta_2O_5 NTs in a tube furnace at 800 °C under an NH_3 gas flow of 100 mL min^{-1} for 3 h. The Ta_2O_5 NTs was prepared by anodizing a Ta foil at 20 V in a mixed solution of glycerol and ethylene glycol (5 vol %) containing 0.2 M NH_4F and 0.15 M $(NH_4)_2SO_4$.

with a potential sweep from −0.1 to 0.7 V versus Ag/AgCl at a scan rate of 20 mV/s. The photocurrent of Ta_3N_5 NTs/Co_3O_4 increased by 3.6 times relative to that of Ta_3N_5 NTs alone under irradiation at 0.6 V versus Ag/AgCl in 0.1 M Na_2SO_4 solution (pH 11). This was attributed to the contribution of Co_3O_4 as an electrocatalyst for water oxidation. Note that, similar to IrO_2, Co_3O_4 showed an improvement as a cocatalyst for Ta_3N_5 NTs for water oxidation. This is an encouraging result given the abundant reserves of Co on the earth.

PEC Measurements of Ta_3N_5 NTs/Co-Pi. Recently, Co-Pi has attracted considerable attention as an effective electrocatalyst for water oxidation.[32,44] To further investigate electrocatalysts based on the earth-abundant Co, Co-Pi was prepared by electrochemical deposition on Ta_3N_5 NTs as described in the Experimental Section. The comparison of LSVs of Ta_3N_5 NTs and Ta_3N_5 NTs/Co-Pi in 0.1 M Na_2SO_4 solution (pH 11) is shown in part c of Figure 6. Co-Pi modification can also improve water oxidation on Ta_3N_5 NTs photoanodes. The photocurrent of Ta_3N_5 NTs/Co-Pi is 2.5 times higher than that of Ta_3N_5 NTs alone. The results in Figure 6 indicate that both cobalt oxide and cobalt phosphate have positive electrocatalytic effects for anodic photocurrent on Ta_3N_5 NTs electrode. The LSV of a Ta_3N_5 NTs/Co-Pi electrode showed a higher photocurrent and a higher electron−hole pair recombination rate (as manifested by the anodic and cathodic current spikes observed under chopped light irradiation) at potentials negative of 0.4 V relative to a Ta_3N_5 NTs/Co_3O_4 electrode. Note also that the latter has somehow higher anodic photocurrents than the former at potentials positive of 0.6 V. These results indicate that Co_3O_4 and Co-Pi have different catalytic activity on Ta_3N_5 NTs and may very likely involve different Co active centers, for example Co(II), Co(III), or higher Co oxidation states in their virginal states.

PEC Measurements of Ta_3N_5 NTs/Pt. Pt modification of Ta_3N_5 NTs was also investigated because Pt was suggested to be an effective electrocatalyst for water oxidation in electrochemical systems.[45,46] Pt NPs were prepared by reducing H_2PtCl_6 precursor in the presence of sodium citrate as described in the Experimental Section. The average diameter of Pt NPs obtained was around 4 nm (Figure S5 of the Supporting Information). Part d of Figure 6 shows the LSVs of Ta_3N_5 NTs and Ta_3N_5 NTs/Pt in 0.1 M Na_2SO_4 solution (pH 11) under chopped irradiation. Ta_3N_5 NTs/Pt showed lower photocurrents than the Ta_3N_5 NTs without electrocatalysts. We also directly deposited Pt on Ta_3N_5 NTs by a photoreduction method.[27] The Ta_3N_5 NTs was immersed in 2 mM H_2PtCl_6 in 0.2 M methanol aqueous solution and light irradiation was performed on the film for 30 min using the Xe lamp. The resulting Ta_3N_5 NTs/Pt film was then rinsed with copious amounts of DI water and tested for PEC water oxidation under the same conditions. No notable improvement in the photocurrent was observed, indicating that Pt was not an effective cocatalyst for Ta_3N_5.

IPCE Measurements. In the above PEC tests on Ta_3N_5 NTs electrodes modified with electrocatalysts, Ta_3N_5 NTs/IrO_2 and Ta_3N_5 NTs/Co_3O_4 showed higher photocurrents for water oxidation. For comparison, the IPCE measurements of Ta_3N_5 NTs/IrO_2, Ta_3N_5 NTs/Co_3O_4 and unmodified Ta_3N_5 NTs were performed under monochromatic light irradiation in 0.1 M Na_2SO_4 aqueous solution (pH 11) at an applied potential of 0.6 V versus Ag/AgCl. Figure 7 shows the IPCE plots of three photoanodes calculated by the following equation:
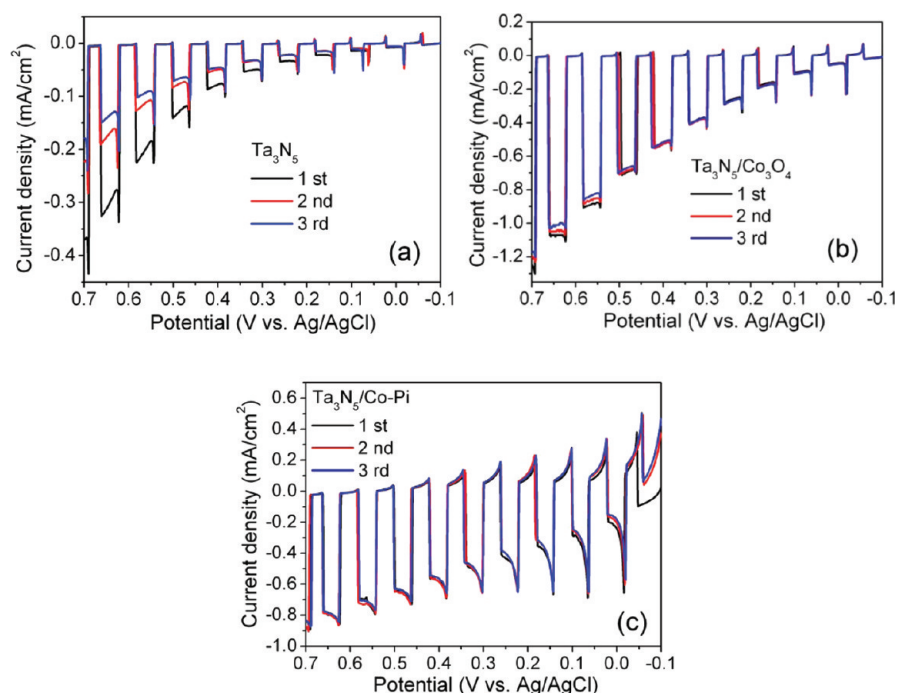

Figure 7. IPCE plots of Ta_3N_5 NTs, Ta_3N_5 NTs/Co_3O_4, and Ta_3N_5 NTs/IrO_2 calculated from the photocurrents in 0.1 M Na_2SO_4 aqueous solution (pH 11) at an applied potential of 0.6 V vs Ag/AgCl.

$$IPCE(\%) = 1240 \times (i_{ph}/\lambda P_{in}) \times 100 \qquad (1)$$

where i_{ph} is the photocurrent (in mA), λ is the wavelength (in nm) of incident radiation, and P_{in} is the incident light power intensity (in mW) on the semiconductor electrode at the selected wavelength. Irradiation at 400 nm (overall white light incident power of the Xe lamp is ∼110 mW/cm^2) Ta_3N_5 NTs/IrO_2 and Ta_3N_5 NTs/Co_3O_4 showed higher IPCE values (∼10% in the best case) relative to an unmodified Ta_3N_5 NT in 0.1 M Na_2SO_4 solution (pH 11) without other redox reagents. The long-wavelength edges of all photocurrent action spectra occurred at 600 nm, suggesting that the band gap of Ta_3N_5 NTs was ca. 2.1 eV and that modification via addition of electrocatalysts did not significantly change the band gap of Ta_3N_5 NTs. These results are consistent with the UV−vis diffuse reflectance spectra of Ta_3N_5 NTs, Ta_3N_5 NTs/IrO_2, and Ta_3N_5 NTs/Co_3O_4 as shown in Figure S6 of the Supporting Information. They also indicate that the obtained photocurrent was generated by a band gap transition of Ta_3N_5 NTs, Ta_3N_5 NTs/IrO_2, and Ta_3N_5 NTs/Co_3O_4.

Stability. Modification with electrocatalysts is expected to improve the stability of the photoanodes because Ta_3N_5 is unstable in photo water oxidation as a result of the self-oxidation of Ta_3N_5 by photogenerated holes.[43] In view of the abundance of Co in the earth's crust, effects of Co_3O_4 and Co-Pi modification on the stability were investigated as the representatives of electrocatalysts. Figure 8 shows a comparison of LSVs of Ta_3N_5 NTs, Ta_3N_5 NTs/Co_3O_4, and Ta_3N_5 NTs/Co-Pi in 0.1 M Na_2SO_4 aqueous solution (pH 11) under chopped irradiation. LSVs of the same samples were repeated three times under the same conditions. The photocurrent of Ta_3N_5 NTs decayed rapidly by 42% in a second sweep indicating instability of Ta_3N_5. For Ta_3N_5 NTs/Co_3O_4 and Ta_3N_5 NTs/Co-Pi photoanodes, the photocurrent remained stable in the second (or third) sweep. This indicates that the modification of cobalt oxide/phosphate improves water oxidation and suppresses the decomposition of the Ta_3N_5 NTs. More quantitative measurements on the faradaic efficiencies of various photoelectrodes for water photooxidation are described below.

Tip Collection/Substrate Generation Measurements. SECM was used to detect the oxygen generated from Ta_3N_5 electrodes under light irradiation. A ring-disk electrode (RDE) coated around the fiber optic was used as the tip electrode as shown in Figure S7 of the Supporting Information. The optical fiber has a diameter of 200 μm and a doped SiO_2 clad surrounding the optical fiber had a thickness of 10 μm. Au was

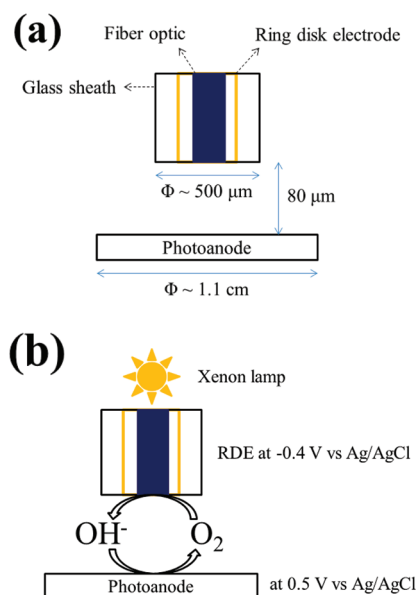**Figure 8.** LSVs of Ta$_3$N$_5$ NTs (a), Ta$_3$N$_5$ NTs/Co$_3$O$_4$ (b), and Ta$_3$N$_5$ NTs/Co-Pi (c), in 0.1 M Na$_2$SO$_4$ aqueous solution (pH 11) under chopped irradiation. Scan rate: 20 mV/s. Light intensity: 110 mW/cm^2 (150 W Xe lamp). Ta$_3$N$_5$ NTs were prepared by nitriding a Ta$_2$O$_5$ NTs anodized at 20 V in the tube furnace at 800 °C under an NH$_3$ gas flow of 100 mL min^{-1} for 3 h.

coated around the SiO$_2$ with a thickness of about 20 μm, finally a borosilicate glass sheath borosilicate glass sheath coats the Au RDE. The outer diameter of the RDE/fiber optic tip was about 500 μm (as shown in part c of Figure S7 of the Supporting Information).

Part a of Figure S8 of the Supporting Information shows a cyclic voltammogram (CV) of the Au RDE in a 1 mM ferrocenemethanol (FcMeOH) and 0.1 M KCl solution. The current obtained from the RDE in the SECM configuration is a function of (a) the outer ring radius, (b) the ratio of inner and outer ring electrode radii, and (c) the ratio of outer glass sheath and the outer ring electrode radii (Rg).[47] Here, the ratio of inner and outer ring radii was about 0.92 (or 220 μm/240 μm) and Rg was about 2.1 (or 500 μm/240 μm). The current measured from RDE at long distance from the substrate was a little larger than that obtained from the numerical simulation (Figure S9 of the Supporting Information), which may imply a small deviation of the electrode area from that defined in the simulation. However, the RDE coated around the fiber optic was successfully prepared and no severe leakage current was observed that can impede the TC/SG measurements.

To detect oxygen by the oxygen reduction reaction (ORR), the RDE was modified and Pt was deposited on a Au RDE to promote the ORR, since this reaction is slow on a Au electrode and a fast reaction is required for diffusion limited TC in SECM. Pt was deposited from a 10 mM H$_2$PtCl$_6$ and 0.1 M Na$_2$SO$_4$ aqueous solution by repeated cyclic voltammetry from 0.2 V to −0.7 V (vs Ag/AgCl) for three scans at a rate of 20 mV/s. The Pt RDE shows distinctive proton reduction peaks which is not observed at a Au RDE as shown in part b of Figure S8 of the Supporting Information.
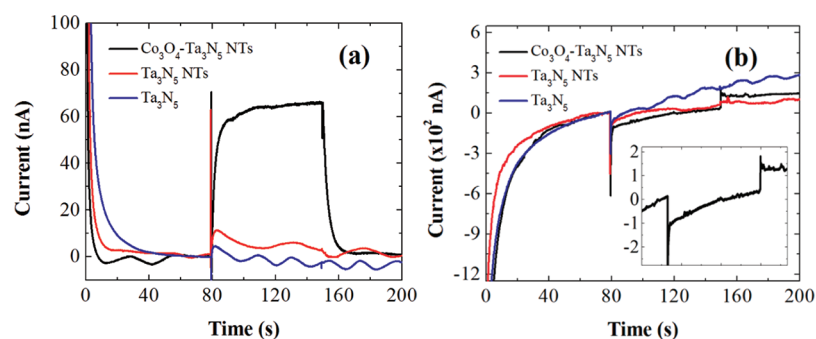
The schematic diagram shown in Figure 9 illustrates the electrode configuration of the TC/SG mode of SECM. The Pt RDE/fiber optic was placed a few tens of μm above the photoanode substrate. A positive potential was applied to the

Figure 9. Schematic diagram of the TC/SG mode of SECM for (a) the electrode configuration and (b) showing the electrochemical reactions in which water oxidation occurs at a photoanode under irradiation, i.e., substrate generation with oxygen reduction at the Pt ring electrode.

photoanode to promote the OER and a negative potential was applied to the Pt RDE for the ORR. Then, the photoanode was irradiated with a xenon lamp via the RDE and the currents of both the tip and the substrate were measured to calculate the collection efficiency, that is, the ratio of the tip (collection) current and the substrate (generation) current.

The collection efficiency is a function of the electrode geometry and the distance between the tip and substrate, *d*. In

Figure 10. Chronoamperograms of (a) tip collection and (b) substrate generation for water oxidation on $Co_3O_4-Ta_3N_5$ nanotubes (black), Ta_3N_5 nanotubes (red), and Ta_3N_5 (blue) electrodes in a 0.1 M Na_2SO_4 and 1 mM KOH (pH 11) aqueous solution. The measurements began in the dark and the UV−vis irradiation was switched on with the full output of the xenon lamp from 80 to 150 s. As the radiation started, oxygen evolution current begins and the generation current on the electrode is about 100 nA at 150 s for the $Co_3O_4-Ta_3N_5$ electrode (b, black). The generated oxygen diffused to the Pt-RDE where oxygen reduction reaction occurs. The collected current from oxygen reduction is about 60 nA at 150 s (a, black). Absolute collection efficiency (the ratio between the generation current and the collection current) is about 60%. The potential of the $Co_3O_4-Ta_3N_5$ nanotube electrode was held at 0.5 V and that of Pt-RDE was held at −0.4 V. Inset in (b) is an enlarged figure to clearly show the generation current values from a $Co_3O_4-Ta_3N_5$ nanotube electrode.

general, a higher collection efficiency is expected with a smaller d because less species produced at the substrate is lost to the bulk solution through diffusion. As shown in Figure S10 of the Supporting Information, the results from the numerical calculation show that a theoretical collection efficiency (η_{th}) of 0.68 is obtained at $d = 80$ μm and about 0.90 at $d = 20$ μm. In addition to the higher η_{th}, a short diffusion time, that is, time required for the produced species at the substrate to reach the tip to be collected, can be achieved with a small d as indicated by the equation described below.

$$d^2 = 2Dt \qquad (2)$$

where d is the tip−substrate distance in cm, D is the diffusion coefficient in cm^2/s, and t is the diffusion time in s. When $d = 20$ μm, the diffusion time is about 100 ms with an oxygen diffusion coefficient of 2×10^{-5} cm^2/s.[48]

When an n-type semiconductor is used as the substrate, it is considered as a conductive electrode under strong light irradiation as the photooxidation occurs. However, the conductive area of the photoanode is only confined to the irradiated region and the rest of the semiconductor is still insulating. Consequently, when the RDE is used as the tip, the irradiated area under the fiber optic is changed when the tip−substrate distance changes, that is the area of the light distribution increases with d. The light distribution area can be calculated using the acceptance angle of the fiber optic, that is, the angle in the fiber optic below which the light is spread. The acceptance angle of RDE/fiber optic used was 25°.

As discussed above, the theoretical collection efficiency (η_{th}) approaches 0.90 as the distance between the tip and the substrate decreases. Although the assumption on diffusion-limited substrate generation current is not fully satisfied due to the slow OER kinetics on the electrocatalyst at a pH less than 13,[49] it should not affect the constant flux assumption of the product generated from the substrate in the theoretical simulation of the OER at the photoanode. The generation current also decreases for the decreased area. Note that the illumination intensity was assumed to be strong enough that the simulated photocurrent from the substrate depended only on the irradiated area. In the TC/SG mode of SECM, a RDE/fiber optic was placed at 80 μm above the photoanode using a linear actuator (T-LA28A, Zaber Technologies Inc., Vancouver,

Canada) to achieve both the large generation/collection current and reasonable collection efficiency (part a of Figure 9).

A W/Mo-doped $BiVO_4$ photoanode was first used as a standard to examine the TC/SG mode SECM. W/Mo-doped $BiVO_4$ has been reported to be a highly active and stable photoanode for water oxidation.[50] Briefly, W/Mo-doped $BiVO_4$ was placed in a 0.1 M Na_2SO_4 aqueous solution (pH 7, 0.2 M sodium phosphate buffer). Then, the RDE/fiber optic was placed 80 μm above the substrate as discussed above. The potential applied to the RDE was −0.2 V and to the photoanode 0.5 V versus Ag/AgCl to promote the ORR and OER, respectively. Chronoamperograms of the RDE/photoanode are shown in Figure S11 of the Supporting Information. When the light was turned on at 80 s, the oxidation current at the W/Mo-doped $BiVO_4$ increased rapidly for the water oxidation. The generated oxygen diffused to the tip and was reduced at the Pt RDE. The collected current also rapidly increased as shown in part a of Figure S11 of the Supporting Information. The measured collection efficiency was about 0.60 which agrees well with the numerical simulation as discussed above with about a $d = 80$ μm. In summary, the TC/SG mode of SECM was demonstrated with a W/Mo-BiVO$_4$ substrate and Pt RDE/fiber optic to detect the oxygen generated at the photoanode.

The water oxidation at $Co_3O_4-Ta_3N_5$ NTs, Ta_3N_5 NTs, and Ta_3N_5 electrodes were also studied using the TC/SG mode of SECM as shown in Figure 10. Chronoamperograms were measured in a 0.1 M Na_2SO_4 and 1 mM KOH aqueous solution (pH 11). The $Co_3O_4-Ta_3N_5$ NT electrode showed a much higher photoactivity than the Ta_3N_5 NTs and Ta_3N_5 films, as discussed in Figures 4 and 6. The oxidation currents obtained at the photoanode was about ($Co_3O_4-Ta_3N_5$ NTs) 100 nA, (Ta_3N_5 NTs), 60 nA, and (Ta_3N_5 film) 30 nA at 0.5 V (vs Ag/AgCl) under irradiation (part b of Figure 10). The collected current at the RDE was about 60 nA for the $Co_3O_4-Ta_3N_5$ NTs or a collection efficiency of about 0.60 based on the quasi-steady-state current at 150 s. The collection efficiency measured from $Co_3O_4-Ta_3N_5$ NTs was close to that obtained with W/Mo-BiVO$_4$ and from the numerical simulations, as shown in Figures S10 and S11 of the Supporting Information at the identical tip/substrate distance. Also, there was no other species that can be reduced at the RDE except for oxygen. Thus, the collected current implies that after correcting for the theoretical

14548

dx.doi.org/10.1021/jp304340a | J. Phys. Chem. C 2012, 116, 14541−14550

collection efficiency (0.68 at distance 80 μm), at least 88% of the oxidation current at Co_3O_4–Ta_3N_5 NTs is from water oxidation.

However, the collected current above Ta_3N_5 NTs and Ta_3N_5 photoanodes was about 10 nA and less than 5 nA, respectively, as shown in part a of Figure 10 and the corresponding collection efficiency for both Ta_3N_5 NTs and Ta_3N_5 was less than 0.15. The significantly smaller collection efficiencies for Ta_3N_5 NTs and Ta_3N_5 than that obtained from Co_3O_4–Ta_3N_5 NTs (or W/Mo-doped $BiVO_4$) indicate that the current efficiency for water oxidation at the Ta_3N_5 NTs and Ta_3N_5 is far less than that of Co_3O_4–Ta_3N_5 NTs. As discussed above, oxidation of the nitride film has been reported and the Ta_3N_5 NTs and Ta_3N_5 film are probably oxidized by the photo-generated holes. The results obtained from the TC/SG mode of SECM agree with those from Figure 8 that electrocatalysts suppress this oxidation of the nitride electrodes and improves the stability of the Ta_3N_5 films. Note that the collected current at the RDE and the collection efficiency are sensitive to d and the electrode configuration. However, in part a of Figure 10, the rapid increase of the tip current at 80 s for all of the Ta_3N_5 films indicates that the RDE was properly located with respect to the photoanode at small d. Thus, the low collection efficiencies at Ta_3N_5 NTs and Ta_3N_5 did not originate from experimental error, for example, misplacement of the tip above the substrate, but rather from the low current efficiency as discussed above. However, even Co_3O_4–Ta_3N_5 NTs are not completely stable, as reported previously,[51] and the stability problem of nitrides needs to be addressed in future studies.

CONCLUSIONS

Ta_3N_5 NTs have been successfully fabricated by electrochemical anodization of a Ta foil followed by ammonia treatment at 800 °C. The obtained Ta_3N_5 NTs were uniform and highly oriented. The main phase of the Ta_3N_5 NTs was identified to be orthorhombic. Nanostructured Ta_3N_5 showed a photocurrent more than 3 times higher than a regular Ta_3N_5 film in 0.1 M Na_2SO_4 aqueous solution (pH 11). IrO_2 NPs, Co_3O_4 NPs, Co-Pi, and Pt NPs were used as cocatalysts to modify the surface of Ta_3N_5 NTs to decrease the activation energy for water oxidation. IrO_2, Co_3O_4, and Co-Pi showed a positive improvement for PEC water oxidation on Ta_3N_5 NTs, whereas Pt was ineffective. The photocurrents of Ta_3N_5 NTs/IrO_2 and Ta_3N_5 NTs/Co_3O_4 were ca. four times higher than that of Ta_3N_5 NTs alone. The IPCE values of Ta_3N_5 NTs/IrO_2 and Ta_3N_5 NTs/Co_3O_4 photoanodes were ~10% at 400 nm irradiation at 110 mW/cm^2 in 0.1 M Na_2SO_4 aqueous solution (pH 11). Cobalt oxide and cobalt phosphate are promising candidates as electrocatalysts for Ta_3N_5 for water oxidation given the abundance of Co in the earth's crust. SECM was employed to study the faradaic efficiency of Co_3O_4–Ta_3N_5 NTs, Ta_3N_5 NTs, and Ta_3N_5 electrodes for water oxidation. Tip collection/substrate generation measurements show that the oxidation current from Co_3O_4–Ta_3N_5 NTs was mostly from water oxidation. However, the nitride films without electrocatalysts, for example, Ta_3N_5 NTs and Ta_3N_5, significantly suffered from self-oxidation of nitride by the photogenerated holes. In summary, the cobalt oxide not only improves the photoactivity of Ta_3N_5 for water oxidation but is also important to the nitride photoanode to decrease the rate of degradation.

ASSOCIATED CONTENT

Ⓢ Supporting Information

Additional experimental data and figures. This material is available free of charge via the Internet at http://pubs.acs.org.

AUTHOR INFORMATION

Corresponding Author
*E-mail: ajbard@mail.utexas.edu.

Present Address
[†]College of Environmental Science and Engineering, Zhejiang Gongshang University, Hangzhou, 310012, China.

Author Contributions
[‡]These authors contributed equally to this work.

Notes
The authors declare no competing financial interest.

REFERENCES

(1) Yin, Q. H.; Tan, J. M.; Besson, C.; Geletii, Y. V.; Musaev, D. G.; Kuznetsov, A. E.; Luo, Z.; Hardcastle, K. I.; Hill, C. L. *Science* **2010**, *328*, 342−345.
(2) Fujishima, A.; Honda, K. *Nature* **1972**, *238*, 37−38.
(3) Nah, Y. C.; Paramasivam, I.; Schmuki, P. *Chem. Phys. Chem.* **2010**, *11*, 2698−2713.
(4) Khan, S. U. M.; Al-Shahry, M.; Ingler, W. B. *Science* **2002**, *297*, 2243−2245.
(5) Park, J. H.; Kim, S.; Bard, A. J. *Nano Lett.* **2006**, *6*, 24−28.
(6) Yang, H. G.; Sun, C. H.; Qiao, S. Z.; Zou, J.; Liu, G.; Smith, S. C.; Cheng, H. M.; Lu, G. Q. *Nature* **2008**, *453*, 638−641.
(7) Chen, X. B.; Liu, L.; Yu, P. Y.; Mao, S. S. *Science* **2011**, *331*, 746−750.
(8) Kudo, A.; Miseki, Y. *Chem. Soc. Rev.* **2009**, *38*, 253−278.
(9) Yokoyama, D.; Hashiguchi, H.; Maeda, K.; Minegishi, T.; Takata, T.; Abe, R.; Kubota, J.; Domen, K. *Thin Solid Films* **2011**, *519*, 2087−2092.
(10) Zhang, Q. H.; Gao, L. *Langmuir* **2004**, *20*, 9821−9827.
(11) Abe, R.; Higashi, M.; Domen, K. *J. Am. Chem. Soc.* **2010**, *132*, 11828−11829.
(12) Ishikawa, A.; Takata, T.; Kondo, J. N.; Hara, M.; Domen, K. *J. Phys. Chem. B* **2004**, *108*, 11049−11053.
(13) Tabata, M.; Maeda, K.; Higashi, M.; Lu, D. L.; Takata, T.; Abe, R.; Domen, K. *Langmuir* **2010**, *26*, 9161−9165.
(14) Hara, M.; Hitoki, G.; Takata, T.; Kondo, J. N.; Kobayashi, H.; Domena, K. *Catal. Today* **2003**, *78*, 555−560.
(15) Maeda, K.; Nishimura, N.; Domen, K. *Appl. Catal. A-Gen.* **2009**, *370*, 88−92.
(16) Hitoki, G.; Ishikawa, A.; Takata, T.; Kondo, J. N.; Hara, M.; Domen, K. *Chem. Lett.* **2002**, *7*, 736−737.
(17) Feng, X. J.; LaTempa, T. J.; Basham, J. I.; Mor, G. K.; Varghese, O. K.; Grimes, C. A. *Nano Lett.* **2010**, *10* (3), 948−952.

(18) Zhu, K.; Neale, N. R.; Miedaner, A.; Frank, A. J. *Nano Lett.* **2007**, *7*, 69−74.

(19) Ghicov, A.; Aldabergenova, S.; Tsuchyia, H.; Schmuki, P. *Angew. Chem., Int. Ed.* **2006**, *45*, 6993−6996.

(20) Grimes, C. A. *J. Mater. Chem.* **2007**, *17*, 1451−1457.

(21) Mohapatra, S. K.; John, S. E.; Banerjee, S.; Misra, M. *Chem. Mater.* **2009**, *21*, 3048−3055.

(22) Rangaraju, R. R.; Raja, K. S.; Panday, A.; Misra, M. *Electrochim. Acta* **2010**, *55*, 785−793.

(23) Wei, W.; Macak, J. M.; Shrestha, N. K.; Schmuki, P. *J. Electrochem. Soc.* **2009**, *156*, K104−K109.

(24) Banerjee, S.; Mohapatra, S. K.; Misra, M. *Chem. Commun.* **2009**, *46*, 7137−7139.

(25) Roy, P.; Das, C.; Lee, K.; Hahn, R.; Ruff, T.; Moll, M.; Schmuki, P. *J. Am. Chem. Soc.* **2011**, *133*, 5629−5631.

(26) Mor, G. K.; Prakasam, H. E.; Varghese, O. K.; Shankar, K.; Grimes, C. A. *Nano Lett.* **2007**, *7*, 2356−2364.

(27) Ye, H.; Park, H. S.; Bard, A. J. *J. Phys. Chem. C* **2011**, *115*, 12464−12470.

(28) Nakagawa, T.; Beasley, C. A.; Murray, R. W. *J. Phys. Chem. C* **2009**, *113*, 12958−12961.

(29) Kuwabara, T.; Tomita, E.; Sakita, S.; Hasegawa, D.; Sone, K.; Yagi, M. *J. Phys. Chem. C* **2008**, *112*, 3774−3779.

(30) Esswein, A. J.; McMurdo, M. J.; Ross, P. N.; Bell, A. T.; Tilley, T. D. *J. Phys. Chem. C* **2009**, *113*, 15068−15072.

(31) Dong, Y. M.; He, H.; Yin, L.; Zhang, A. M. *Nanotechnology* **2007**, *18*, 435602.

(32) Kanan, M. W.; Nocera, D. G. *Science* **2008**, *321*, 1072−1075.

(33) Surendranath, Y.; Kanan, M. W.; Nocera, D. G. *J. Am. Chem. Soc.* **2010**, *132*, 16501−16509.

(34) Tsuji, E.; Imanishi, A.; Fukui, K.; Nakato, Y. *Electrochim. Acta* **2011**, *56*, 2009−2016.

(35) Fang, Y. H.; Liu, Z. P. *J. Am. Chem. Soc.* **2010**, *132*, 18214−18222.

(36) Kiwi, J.; Grätzel, M. *Angew. Chem., Int. Ed.* **1978**, *17*, 860−861.

(37) Fuentes, R. E.; Farell, J.; Weidner, J. W. *Electrochem. Solid State Lett.* **2011**, *14*, E5−E7.

(38) Kibria, M. F.; Mridha, M. S. *Int. J. Hydrogen Energy* **1996**, *21*, 179−182.

(39) Nadesan, J. C. B.; Tseung, A. C. C. *J. Electrochem. Soc.* **1985**, *132*, 2957−2959.

(40) Jiao, F.; Frei, H. *Angew. Chem., Int. Ed.* **2009**, *48*, 1841−1844.

(41) Xiao, X. Y.; Fan, F.-R. F.; Zhou, J. P.; Bard, A. J. *J. Am. Chem. Soc.* **2008**, *130*, 16669−16677.

(42) Yang, J.; Lee, J. Y.; Too, H. P. *Anal. Chim. Acta* **2006**, *571*, 206−210.

(43) Chun, W. J.; Ishikawa, A.; Fujisawa, H.; Takata, T.; Kondo, J. N.; Hara, M.; Kawai, M.; Matsumoto, Y.; Domen, K. *J. Phys. Chem. B* **2003**, *107*, 1798−1803.

(44) Zhong, D. K.; Cornuz, M.; Sivula, K.; Graetzel, M.; Gamelin, D. R. *Energy Environ. Sci.* **2011**, *4*, 1759−1764.

(45) Kiwi, J.; Grätzel, M. *J. Phys. Chem.* **1984**, *88*, 1302−1307.

(46) Alonsovante, N.; Colell, H.; Stimming, U.; Tributsch, H. *J. Phys. Chem.* **1993**, *97*, 7381−7384.

(47) Lee, Y.; Amemiya, S.; Bard, A. J. *Anal. Chem.* **2001**, *73*, 2261−2267.

(48) Ferrell, R. T.; Himmelblau, D. M. *J. Chem. Eng. Data* **1967**, *12*, 111−115.

(49) Minguzzi, A.; Fan, F.-R. F.; Vertova, A.; Rondininia, S.; Bard, A. J. *Chem. Sci.* **2012**, *3*, 217−229.

(50) Park, H. S.; Kweon, K. E.; Ye, H.; Paek, E.; Hwang, G. S.; Bard, A. J. *J. Phys. Chem. C* **2011**, *115*, 17870−17879.

(51) Cong, Y.; Park, H. S.; Dang, H. X.; Fan, F.-R. F.; Bard, A. J.; Mullins, C. B. *Chem. Mater.* **2012**, *24*, 579−586.